Title

Network Analysis on Predicting Mean Diffusivity Change at Group Level in Temporal Lobe Epilepsy

Journal

Brain Connectivity, 6(8)

ISSN

2158-0014

Authors

Abdelnour, Farras
Raj, Ashish
Devinsky, Orrin
et al.

Publication Date

2016-10-01

DOI

10.1089/brain.2015.0381

Peer reviewed

BRAIN CONNECTIVITY
Volume 6, Number 8, 2016

DOI: 10.1089/brain.2015.0381

Network Analysis on Predicting Mean Diffusivity Change at Group Level in Temporal Lobe Epilepsy

Farras Abdelnour,[1] Ashish Raj,[1] Orrin Devinsky,[2] and Thomas Thesen[2]

Abstract

The two most common types of temporal lobe epilepsy are medial temporal sclerosis (TLE-MTS) epilepsy and MRI-normal temporal lobe epilepsy (TLE-no). TLE-MTS is specified by its stereotyped focus and spread pattern of neuronal damage, with pronounced neuronal loss in the hippocampus. TLE-no exhibits normal-appearing hippocampus and more widespread neuronal loss. In both cases, neuronal loss spread appears to be constrained by the white matter connections. Both varieties of epilepsy reveal pathological abnormalities in increased mean diffusivity (MD). We model MD distribution as a simple consequence of the propagation of neuronal damage. By applying this model on the structural brain connectivity network of healthy subjects, we can predict at group level the MD gray matter change in the epilepsy cohorts relative to a control group. Diffusion tensor imaging images were acquired from 10 patients with TLE-MTS, 11 patients with TLE-no, and 35 healthy subjects. Statistical validation at the group level suggests high correlation with measured neuronal loss ($R = 0.56$ for the TLE-MTS group and $R = 0.364$ for the TLE-no group). The results of this exploratory work pave the way for potential future clinical application of the proposed model on individual patients, including predicting neuronal loss spread, identification of seizure onset zones, and helping in surgical planning.

Keywords: epilepsy; graph theory; networks

Introduction

Epilepsy [recently redefined (Fisher et al., 2014)] is one of the most prevalent neurological disorders. In the United States alone, there are 48 new cases of epilepsy every year for every 100,000. The estimated prevalence of epilepsy is 7.1 per 1000 people (Hirtz et al., 2007). Common types of temporal lobe epilepsy (TLE) are medial temporal sclerosis (TLE-MTS) epilepsy and MRI-normal temporal lobe epilepsy (TLE-no). TLE-MTS is characterized by a pattern of neuronal loss in the hippocampus and an electroclinical syndrome, with widespread extralimbic atrophy seen in many cases. TLE-no has normal-appearing hippocampus on MRI and its epileptogenic area in the temporal lobe is more widespread, less well defined, and often includes both hippocampus and neocortical regions. The hippocampus is the principal epileptogenic focus.

It is now believed, based on ictal EEG signature, that other mesial temporal structures play a key role in triggering a seizure, particularly the entorhinal cortex (Bartolomei et al., 2005). Another key region in the generation of an MTS seizure is the amygdala (Bertram, 2009; Gotman and Levtova, 1996). Some episodes may be generated by the hippocampus, while others may be triggered by the amygdala. Along with the hippocampus, the amygdala often plays a role in MTS (Bertram, 2009; Gotman and Levtova, 1996) and can be the source of seizures. These structures are highly connected, providing significant feedback mechanisms (Staf-strom, 2005), suggesting that local network hyperexcitability may be particularly important in seizure propagation. Mueller and associates (2009) identify cortical thinning in TLE-no subjects in the superior frontal region and identify positive correlation between the superior frontal region and the epileptogenic focus.

In both TLE-MTS and TLE-no, the topographic patterns of neuronal loss appear to occur in regions that are connected to the epileptogenic focus zone through white matter (WM) fiber connections (Concha et al., 2012). An important issue in this context is to understand the neural and network basis underlying these patterns of neuronal loss and the contribution of WM connectivity pathways. The prevalent hypothesis in this regard proposes that a seizure activity propagates outwards from the epileptogenic zone along its fiber connections, and neuronal damage is a consequence of local excitotoxicity (Meldrum, 1993). In this model, the extrahippocampal spread of seizure activity is primarily responsible for the apparent

[1]Department of Radiology, Weill Cornell Medical College, New York, New York.
[2]Department of Neurology, New York University, New York, New York.

topographic distribution of atrophy (Riederer et al., 2008; Spencer, 2002; Sutula et al., 2003). The medial temporal and limbic structures are highly connected to each other, as well as to the hippocampus.

The resulting subnetwork leads to significant feedback mechanisms (Stafstrom, 2005), leading to the spread of initially local epileptogenic activity to widespread connected regions. Since the aberrant hyperactive regions are well-established early in disease, this model would predict that, while atrophy may worsen with time, there is no center-out progression of atrophy. Although neuronal death secondary to sustained hyperactivity is not entirely understood, it likely entails mutual intercortical trophic exchanges, ultimately leading to long-lasting remodeling of brain networks (Bernhardt et al., 2011), followed by excitotoxicity-induced neuronal loss. Recent studies, however, suggest a second mechanism that neuronal loss, and eventually gross atrophy, is a progressive degenerative process triggered at the hyperactive epileptogenic focus by excitotoxicity, and extrafocal neuronal loss is a progressive event as a consequence of a cascade of remote degeneration, deafferentation, and loss of trophic support. This hypothesis has found recent support from studies showing that cortical atrophy in epilepsy often co-occurs with WM degeneration of connected tracts (Concha et al., 2009).

The purpose of this study is to use network theory to determine whether the progressive deafferentation model is supported by neuroimaging data in TLE patients. This is a challenging problem because there is very little longitudinal neuroimaging data of sufficiently long time spans to conclusively demonstrate progressive degeneration in broad brain regions. Furthermore, much of this research is phenomenological and descriptive, hence not well suited for quantitative assessment. Quantitative model development is further hampered by heterogeneity in the topography of the disease among TLE patients. In this study, we propose a mathematical model of progressive neuronal damage as a deafferentation process enacted on the brain's structural connectivity (SC) network.

This model is based on a general class of network diffusion models previously proposed by our laboratory, which assumes that the overall behavior of the complex deafferentation process can be approximately captured by linear low-order differential equations defined on network nodes. Similar models have been proposed and implemented in the areas of signal and image processing (Elmoataz et al., 2008; Shuman et al., 2013; Zhang and Hancock, 2008). Recently, network models applied to brain abnormalities have been published, for example, estimating the profile of functional activity in the brain (Abdelnour et al., 2014), as well as the prediction of the neurodegeneration (Raj et al., 2012).

Using network diffusion as a foundation, we derive the specific dynamic equations governing the evolution of progressive neuronal loss on the brain connectome. Then, we determine whether this model, when applied to brain connectomes derived from diffusion MRI scans, can successfully predict the topographic patterns of neuronal loss seen in 10 TLE-MTS and 11 TLE-no patients. Importantly, we propose that the model's predictions can be tested exclusively using cross-sectional neuroimaging data, without requiring longitudinal follow-up. The reason for this is that, although the network model predicts a dynamic spatiotemporal pattern of neuronal loss that ''radiates'' outward from the focus region, the topography of these patterns is dependent entirely on the network topology, and therefore conserved over large spans of time.

The biomarker of neuronal loss used in this study is the regional *t*-statistics of mean diffusivity (MD) calculated from diffusion tensor imaging (DTI) scans of the TLE-MTS/TLE-no groups versus an age-matched control group (Assaf et al., 2003; Mukherjee et al., 2008; Scanlon et al., 2013). DTI is a noninvasive technique, which measures the direction of water diffusion in brain tissue. Key to DTI's usefulness is the tendency of WM internal fibrous structure to be anisotropic in normal brains, with water diffusing largely in the direction of the internal structure.

Although common DTI metrics such as MD and fractional anisotropy (FA) are typically evaluated in WM rather than gray matter (GM) (Concha et al., 2009), their utility as GM markers is also becoming widespread (Bonilha et al., 2010; Pfefferbaum et al., 2010). MD in particular is especially useful in epilepsy, where gross atrophy measured from structural MRI is frequently too insensitive to capture subtle damage outside the hippocampus. Furthermore, cortical dysplasia is a common feature of epilepsy, which confounds current cortical thickness or volume measures (DuBois et al., 2011; Thesen et al., 2011). In contrast, MD is much more sensitive to microstructural damage, and may be more suitable as a measure of neuronal loss in TLE. MD was used as a biometric for evaluation of GM in multiple sclerosis (Bozzali et al., 2002), and a consistent relationship between GM volumetrics and FA abnormalities was reported in Keller and associates (2012) and Bonilha and associates (2010). In Assaf and associates (2003), the authors use MD and FA to lateralize TLE-MTS seizure focus at group level as well as individual patients. They additionally conclude that MD is superior to FA in identifying the epileptogenic focus in GM. In a related work, Concha and associates (2009) studying both TLE-MTS and TLE-no, the authors conclude that, while some regions are affected equally in both TLE types relative to control group, they appear to have distinct extratemporal abnormalities.

Results

We next discuss the results of estimating TLE-MTS and TLE-no group change in MD (D_{av}) relative to normal subjects as an indirect measure of neuronal loss. All named regions are understood to be from the ipsilateral hemisphere, unless otherwise specified. For all figures, the lobes are colored for ease of reading as follows: blue is the frontal lobe, magenta is the parietal lobe, green is the occipital lobe, red refers to the temporal lobe, and cyan refers to the subcortical region. For both TLE-MTS and TLE-no, subjects' D_{av} maps were computed and the GM projected on a 90-region SPM atlas. The subjects were grouped into ipsilateral and contralateral, by side-flipping one group, so that all patients are left-ipsilateral.

We estimate the distribution of graph diffusion that most closely resembles the *t*-statistics obtained from the MTS/TLE-no versus healthy D_{av}. We evaluate the Pearson correlation R between the obtained *t*-statistics and Φ (Equation (7)) over a range of t when a given region is seeded. The process is repeated over all regions. For each region, we choose the graph diffusion yielding the highest R as the diffusion pattern most likely to match the *t*-statistics (and thus the neuronal loss distribution). To take into account the multiple

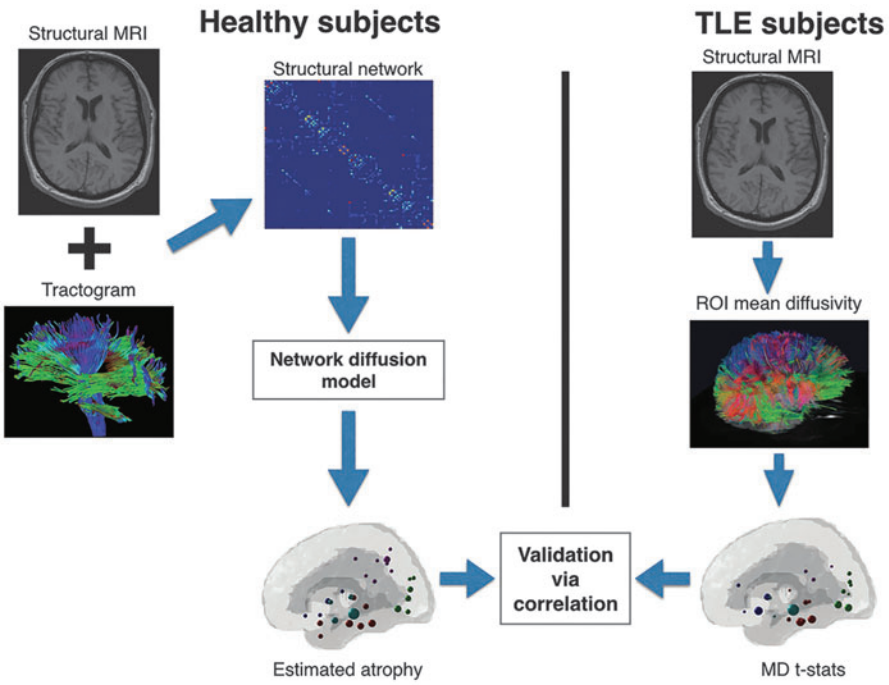

FIG. 1. Flowchart summarizing the proposed methodology. Structural networks are obtained from healthy subjects, then cortical/subcortical atrophies are predicted from the graph diffusion model. Predicted atrophy is then compared with the atrophy patterns obtained from the TLE subjects. TLE, temporal lobe epilepsy. Color images available online at www.liebertpub.com/brain

comparison problem, we use the Benjamini and Hochberg false discovery rate algorithm (Ashby, 2011). We report both the probability of false positive p and the corrected probability p_{fdr}. Figure 1 provides an overview of the datasets and processing steps, as well as the model implementation and evaluation.

TLE-MTS mean diffusivity

Figure 2a gives the t-statistics of the TLE-MTS versus control groups. As expected, the pronounced change in MD, D_{av}, (t-stats >2 std) is found in the ipsilateral hippocampus (6.09 std, $p = 2.7 \times 10^{-7}$, $p_{fdr} = 2.43 \times 10^{-5}$), implying

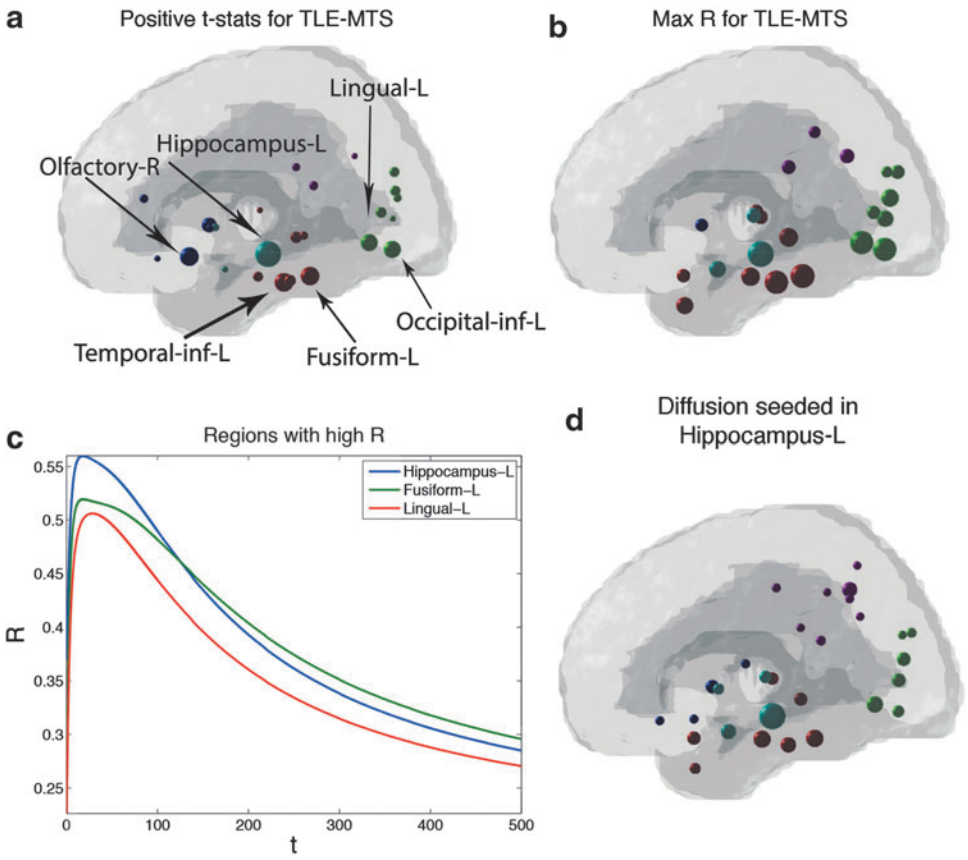

FIG. 2. TLE-MTS: positive t-statistics, **(a)**; the maximum R obtained by placing a seed over each node, **(b)**; Curve of Pearson correlation R obtained over a range of t values, with the curves of the nodes giving the second and third largest R (fusiform and inferior temporal) **(c)**. Diffusion from ipsilateral hippocampus at maximum R with the t-statistics **(d)**; Maximum R is obtained at $t = 14{:}68$, with $R = 0{:}561$. MTS, medial temporal sclerosis. Color images available online at www.liebertpub.com/brain

neuronal loss. Elsewhere, ipsilateral change in D_{av} is found in the frontal lobe (insular gyrus), the occipital lobe (inferior gyrus), and the temporal lobe (parahippocampal). Change in D_{av} relative to normal subjects is additionally found in the contralateral hemisphere in the frontal lobe (olfactory bulb, anterior cingulum gyrus), the parietal lobe (postcingulum), and the occipital lobe (calcarine sulcus and cuneus). Bilateral increase in D_{av} is found in the occipital lobes (lingual, middle occipital, and fusiform gyri) and temporal lobe (middle and inferior gyri).

Figure 2b gives the highest R obtained when a graph diffusion is seeded at each node. Seeding in the ipsilateral hippocampus gives the highest Pearson correlation ($R=0.560$, $p=9.4\times10^{-9}, p_{fdr}=8.50\times10^{-7}$) of all seedings, making it the likely epileptogenic focus. Given these are MTS subjects, this result would appear to agree with the likely role of hippocampus as the onset zone. Other regions yielding high R (>0.5) when seeded (all ipsilateral) are found mainly in the temporal lobe (fusiform and temporal inferior gyrus) and the occipital lobe (lingual and occipital inferior gyri).

The graph diffusion seeded in the ipsilateral hippocampus is given in Figure 2d. The resulting diffusion dominates the ipsilateral GM. The diffusion reaches a maximum at the hippocampus, followed by the fusiform gyrus. The graph diffusion model predicts ipsilateral high D_{av} in the temporal lobe (parahippocampal, and inferior temporal gyri), confirmed in Mueller and associates (2009) and McDonald and associates (2008); the subcortical region (thalamus and amygdala), consistent with Bertram (2009); and the occipital region (lingual gyrus). While the t-statistics in Figure 2a reveals high D_{av} in the contralateral olfactory bulb, it is underestimated by the proposed diffusion model.

We note that when the correlation R of the t-statistics and the estimated atrophy distribution are evaluated only over the ipsilateral hemisphere, we obtain $R=0.707$ ($p=5.9\times10^{-8}$, $p_{fdr}=5.3\times10^{-6}$). Contralateral correlation gives $R=0.449$ ($p=2\times10^{-3}, p_{fdr}=1.1\times10^{-2}$). This is not surprising as the long fibers connecting contralateral/ipsilateral regions tend to be underestimated by the current methods. Across the hemispheres, SC tends to be weaker than within the hemispheres.

Figure 2c depicts R as a function of t for the three nodes yielding the highest R when each node is seeded. When the ipsilateral hippocampus is seeded, the Pearson correlation increases until it reaches a peak of $R=0.560$ at $t=14.68$. Similarly, the fusiform and the lingual gyrus, respectively, reach $R=0.520$ at $t=18.02$ ($p=1.5\times10^{-7}, p_{fdr}=5.7\times10^{-6}$) and $R=0.506$ at $t=28.36$ ($p=3.6\times10^{-7}, p_{fdr}=6.7\times10^{-6}$). In addition, the inferior temporal gyrus has comparable R, with $R=0.506$ at $t=18.24$ ($p=3.7\times10^{-7}, p_{fdr}=6.7\times10^{-6}$).

In Figure 3, we plant a seed in the ipsilateral hippocampus and allow it to diffuse in the network. At $t=1$, the diffusion is largely confined to the subcortical region, in addition to the temporal lobe. Around $t=2.67$, the graph starts diffusing into the parietal and occipital regions. Around diffusion depth $t=8.23$, the diffusion begins to correlate with the D_{av} pattern, reaching a maximum R at $t=14.68$, as described above, and favorably comparing with the t-statistics in Figure 2a.

We investigate the model's performance in the ipsilateral network only. Figure 4a depicts the positive ipsilateral t-statistics. In this case, the graph diffusion is constrained to the ipsilateral cortex only. As shown in Figure 4b, all (ipsilateral) correlation values increase, with the highest R reached once again at the hippocampus, ($R=0.685$, $p=2.1\times10^{-7}$, $p_{fdr}=9.4\times10^{-6}$).

Other ipsilateral regions revealing a higher R include the parahippocampal ($R=0.490$, $p=6.4\times10^{-4}, p_{fdr}=4.2\times10^{-3}$), lingual ($R=0.561$, $p=6.2\times10^{-5}, p_{fdr}=5.6\times10^{-4}$), inferior occipital ($R=0.588$, $p=2.1\times10^{-5}, p_{fdr}=2.4\times10^{-4}$), middle

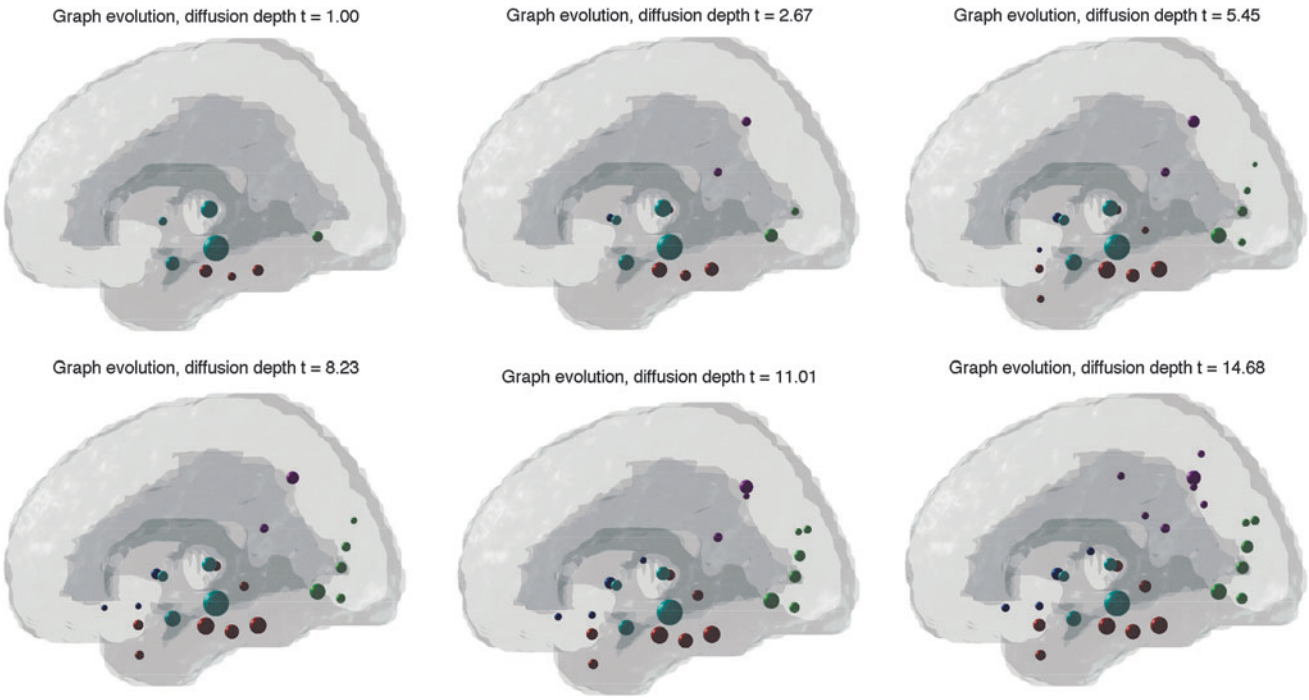

FIG. 3. TLE-MTS: graph evolution when the ipsilateral hippocampus is seeded. Color images available online at www.liebertpub.com/brain

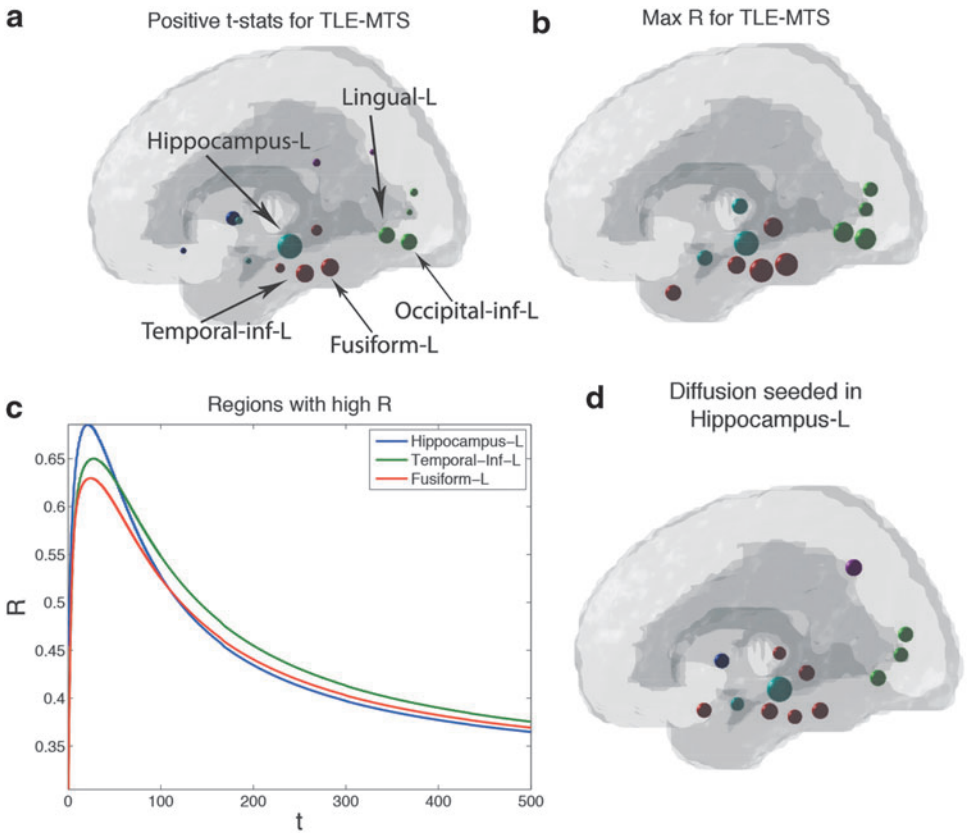

FIG. 4. TLE-MTS: Graph diffusion when only the ipsilateral hemisphere is considered. Ipsilateral positive *t*-statistics **(a)**; *R* when each ipsilateral node is seeded, with maximum *R* resulting from seeding the hippocampus **(b)**; correlation curves for the three nodes giving the highest *R* **(c)**, diffusion from the ipsilateral hippocampus **(d)**. Table 1 lists the 10 nodes with the highest diffusion values. Color images available online at www.liebertpub.com/brain

temporal ($R=0.527, p=1.9\times10^{-4}$, $p_{fdr}=1.5\times10^{-3}$), inferior temporal gyrus ($R=0.650$, $p=1.4\times10^{-6}, p_{fdr}=3.0\times10^{-5}$), and the thalamus ($R=0.438$, $p=2.6\times10^{-3}, p_{fdr}=1.3\times10^{-2}$). The resulting graph diffusion depicted in Figure 4d shows a similarity to the ipsilateral D_{av} map of Figure 4a. Table 1 lists the 10 nodes with the highest network diffusion depicted in Figure 4d. From Figure 4c, the diffusion from the hippocampus reaches a maximum at $t=21.91$. The figure additionally gives the curves of the nodes with the second and third highest *R*, the inferior temporal gyrus and the fusiform (similar to the case of the full network), respectively, given by $R=0.650$ at $t=27.25$ and $R=0.630$ at $t=24.58$.

When we consider the contribution of the individual eigenmodes to the entire network (taking their absolute values), eigenmode $\mathbf{u}_{78}$ gives $R=0.382$ ($p=2.03\times10^{-4}, p_{fdr}=1.8\times10^{-2}$), as given in Figure 5c. Figure 5b reflects eigenmode $\mathbf{u}_{78}$ on the glass brain.

TLE-no mean diffusivity

Similar to the previous Section ''TLE-MTS Mean Diffusivity,'' we compute the graph diffusion on an SC of a representative healthy brain that most closely matches the MD abnormalities in the case of TLE-no.

The *t*-statistics reflecting the MD abnormalities of a group of TLE-no patients compared with a healthy group is depicted in Figure 6a. The peak D_{av} is reached in the occipital region at the contralateral inferior gyrus (t-stats $=3.19\,std$, $p=2.6\times10^{-3}, p_{fdr}=1.2\times10^{-1}$), followed by the contralateral insula (t-stats $=3.06\,std$, $p=3.7\times10^{-3}, p_{fdr}=1.2\times10^{-1}$) and

Table 1. Regions with the Highest Network Diffusion for the TLE-MTS (Left, and Fig. 4), and TLE-no (Right, and Fig. 6) for the Case of 45 Regions (Ipsilateral Hemisphere)

MTS nodes	*MTS diffusion*	*TLE-no nodes*	*TLE-no diffusion*
Hippocampus	1.74	Temporal-Inf	1.63
Precuneus	0.77	Temporal-Mid	0.83
Parahippocampal	0.76	Fusiform	0.77
Fusiform	0.76	Occipital-Mid	0.73
Temporal-Mid	0.73	Occipital-Inf	0.68
Lingual	0.73	Parahippocampal	0.67
Occipital-Mid	0.70	Hippocampus	0.66
Insula	0.68	Temporal-Pole-Sup	0.66
Temporal-Pole-Sup	0.68	Temporal-Pole-Mid	0.64
Calcarine	0.66	Lingual	0.59

TLE-MTS, temporal lobe epilepsy medial temporal sclerosis.

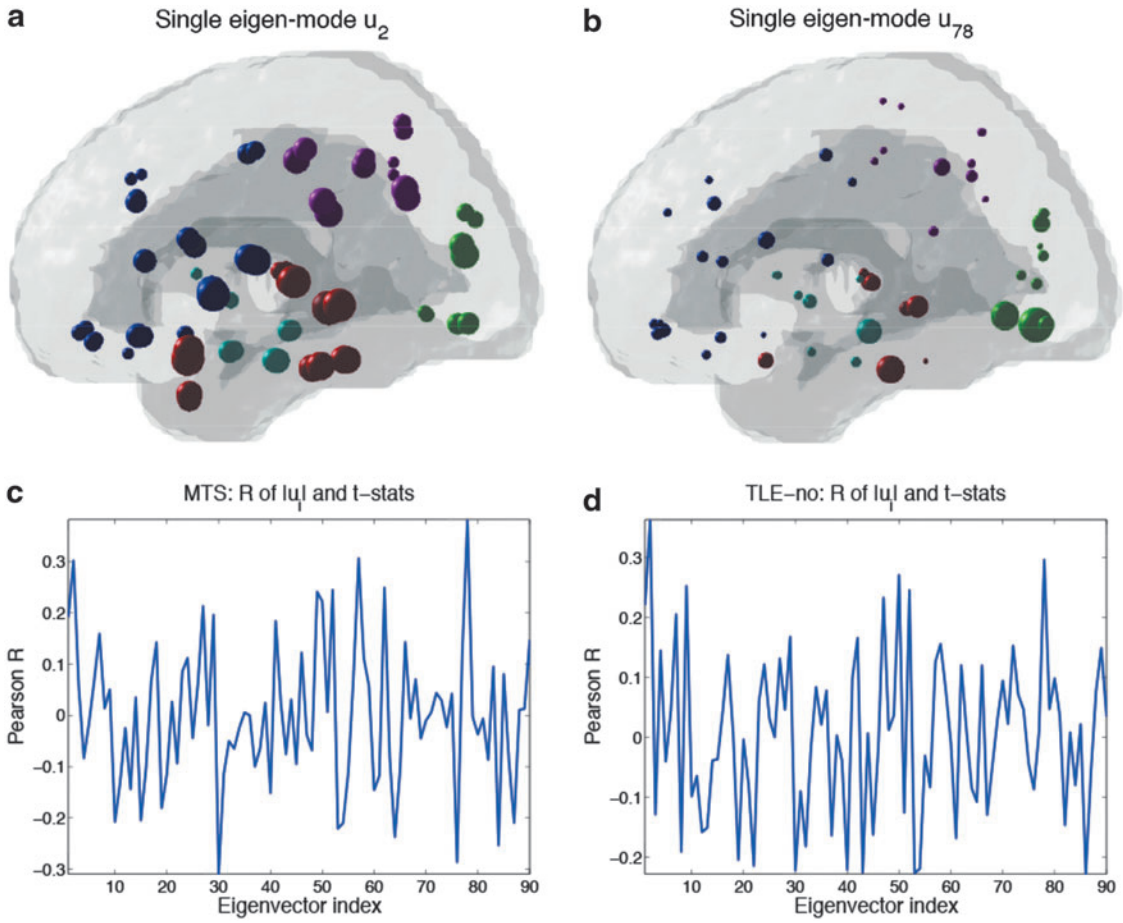

FIG. 5. TLE-no and TLE-MTS as a function of eigenmodes $|\mathbf{u}_i|$. Eigenmode $|\mathbf{u}_2|$ **(a)** captures an approximation of TLE-no t-stats with $R=0.363$ **(c)**. On the other hand $|\mathbf{u}_{78}|$ **(b)** captures an approximation of TLE-MTS t-stats with $R=0.382$ **(d)**. Color images available online at www.liebertpub.com/brain

the ipsilateral temporal inferior gyrus (t-stats $=3.04\,std$, $p=3.9\times10^{-3}, p_{fdr}=1.2\times10^{-1}$). Significant change in D_{av} relative to normal subjects (t-stats >2 std) is found in the (contralateral) frontal lobe (olfactory bulb, anterior cingulum), occipital lobe (calcarine fissure), and parietal lobe (precuneus). Ipsilateral change in D_{av} is found in the subcortical region (hippocampus) and temporal lobe (fusiform). Bilateral increase in D_{av} is found in the frontal lobe (inferior orbital and insula gyri), the occipital lobe (inferior gyri), and the temporal lobe (inferior gyri).

Figure 6b gives the Pearson correlations R when each node is seeded and allowed to diffuse in the structural network. Diffusions seeded in the occipital lobes lead to highest correlations with the t-statistics. Specifically, diffusion from the contralateral calcarine sulcus yields $R=0.364$ ($p=4.2\times10^{-4}$, $p_{fdr}=3.1\times10^{-2}$), followed by the occipital inferior ipsilateral and contralateral gyri ($R=0.341$, $p=10^{-3}$, $p_{fdr}=3.1\times10^{-2}$ and $R=0.349$, $p=7.6\times10^{-4}, p_{fdr}=3.1\times10^{-2}$, respectively). Referring to the t-statistics (Figure 6a), the contralateral calcarine sulcus has one of the more pronounced changes in D_{av} when compared with the healthy group. The contralateral occipital inferior gyrus has the second highest change in D_{av} and shows one of the highest correlations in graph diffusion. In fact, the Pearson correlation between the t-statistics and the vector of maximum correlation for each node yield $R=0.695$ ($p=3\times10^{-14}$).

Figure 6d illustrates the diffusion from the contralateral calcarine sulcus. At the diffusion point of highest correlation with the t-statistics, the graph diffusion is dominated by the calcarine sulcus node, followed bilaterally by the precuneus. Elsewhere, the diffusion stands out in the contralateral middle occipital gyrus. The contralateral hemisphere nodes of the calcarine sulcus diffusion are more strongly correlated to their t-statistics counterparts, with $R=0.475$ ($p=9.8\times10^{-4}, p_{fdr}=1.5\times10^{-2}$), than the ipsilateral hemisphere nodes ($R=0.207$, $p=0.17, p_{fdr}=0.99$). We observe that in this case, when the ipsilateral hemisphere diffusion nodes correlated with the t-statistics counterparts, the highest R is in fact obtained at the inferior temporal node, with $R=0.467$ ($p=1.2\times10^{-3}, p_{fdr}=1.1\times10^{-1}$).

When only the ipsilateral nodes of the left temporal nodes diffusion correlated with the t-statistics counterparts, we obtain $R=0.467$.

The curve of R versus t in Figure 6c shows that the peak R for the contralateral calcarine seeding is reached at $t=59.96$ with $R=0.364$. The second highest correlation results from seeding the contralateral inferior occipital gyrus, yielding $R=0.349$ at $t=99.67$. The ipsilateral hippocampus results in $R=0.286$ at $t=112.13$ ($p=6.3\times10^{-3}, p_{fdr}=4.7\times10^{-2}$) when seeded.

Similar to the TLE-MTS analysis in TLE-MTS Mean Diffusivity Section, we next consider only the nodes spanning

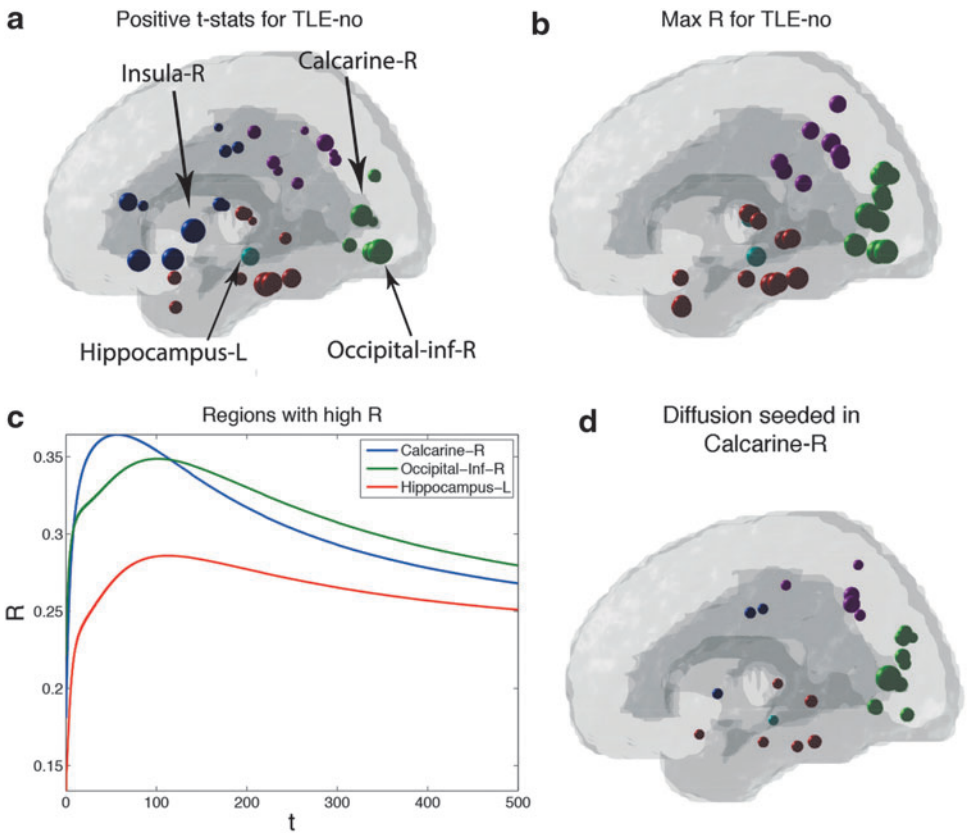

FIG. 6. TLE-no: Positive *t*-statistics, **(a)**; the maximum *R* obtained from seeding all nodes, **(b)**; diffusion from contralateral calcarine gyrus at maximum *R* with the *t*-statistics **(d)**; curve of *R* obtained over a range of *t* values for the contralateral calcarine and occipital inferior, and the ipsilateral hippocampus **(c)**. Highest *R* is obtained when the contralateral calcarine is seeded, with $t = 59.96$ and $R = 0.364$. Color images available online at www.liebertpub.com/brain

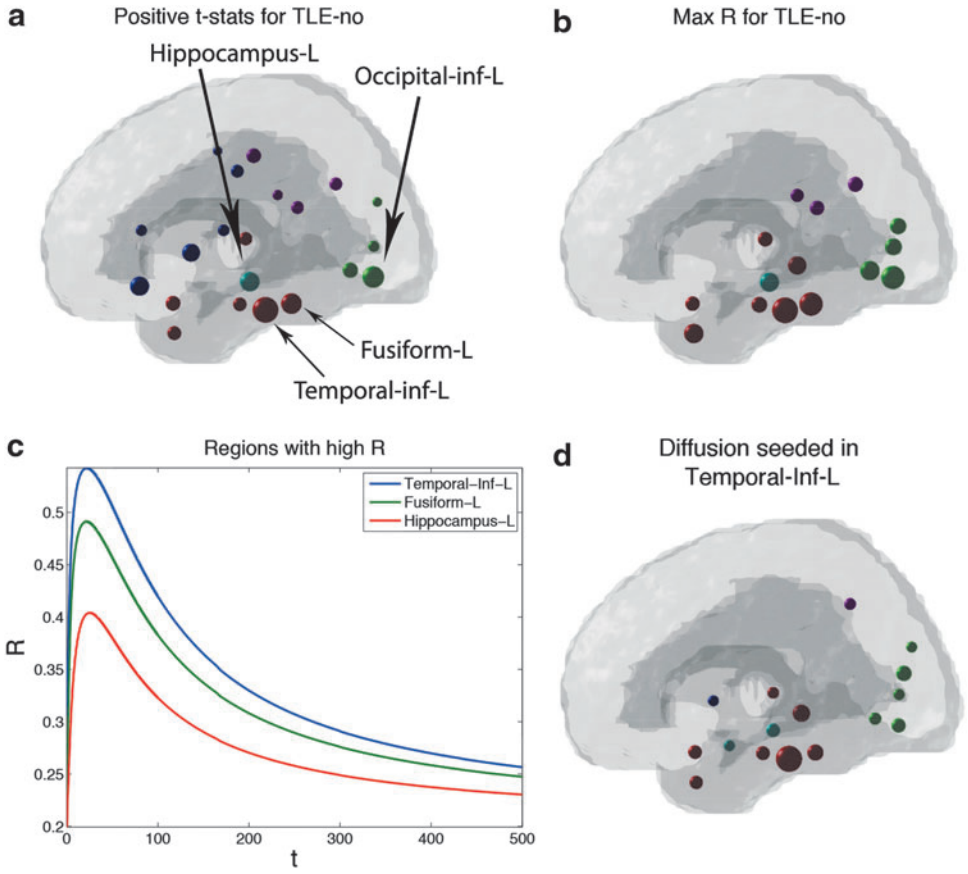

FIG. 7. TLE-no: graph diffusion when only the ipsilateral hemisphere is considered. Ipsilateral positive *t*-statistics **(a)**; *R* when each ipsilateral node is seeded, with maximum *R* resulting from seeding the inferior temporal gyrus ($R = 0.543$) **(b)**; correlation curves for the three nodes giving the highest *R* **(c)**, diffusion from the ipsilateral inferior temporal gyrus **(d)**. Table 1 lists the 10 nodes with the highest diffusion values. Color images available online at www.liebertpub.com/brain

the ipsilateral hemisphere. The ipsilateral hemisphere *t*-statistics is now given in Figure 7a. The correlation due to seeding at each of the hemisphere's nodes is given in Figure 7b. The *R* values now significantly increase, with the ipsilateral inferior temporal gyrus correlating most ($R=0.543$, $p=1.2\times10^{-4}, p_{fdr}=5.3\times10^{-3}$). Other nodes where the corresponding diffusions give high correlations are the occipital inferior, fusiform, and lingual, as well as the hippocampus and the calcarine sulcus. The set of correlations obtained from seeding each node gives a relatively high *R* when correlated with the ipsilateral *t*-statistics vector, with $R=0.725$ and $p=1.8\times10^{-8}$.

Considering the diffusion from the ipsilateral inferior temporal gyrus, given in Figure 7d, it is dominated by the occipital and the temporal lobes, and the hippocampus, with some diffusion in the parietal lobe. Table 1 lists the 10 TLE-no nodes with the highest network diffusion depicted in Figure 7d. The corresponding graph diffusion from the inferior temporal gyrus shows somewhat high value at the precuneus area, even though the inferior temporal gyrus is not directly connected to it. However, the inferior temporal gyrus is structurally strongly connected to the middle temporal gyrus, which in turn is connected to the precuneus.

Figure 7c gives the *R* versus *t* curves for the inferior temporal gyrus ($R=0.543$, $t=21.91$, $p=1.2\times10^{-4}, p_{fdr}=5.3\times10^{-3}$), the fusiform ($R=0.492$, $t=21.91$, $p=6\times10^{-4}, p_{fdr}=9.6\times10^{-3}$), and the hippocampus ($R=0.404$, $t=25.92$, $p=5.9\times10^{-3}, p_{fdr}=4.4\times10^{-2}$).

Once again, considering the contribution of the individual eigenmodes (taking their absolute values) over the full network, eigenmode $\mathbf{u}_2$ gives $R=0.363$ ($p=4.4\times10^{-4}$, $p_{fdr}=4.0\times10^{-2}$), as given in Figure 5d. Figure 5a reflects eigenmode $\mathbf{u}_2$ on the glass brain.

Statistical significance

A *t*-test between the TLE-MTS and TLE-no groups is performed on the correlation value *R* obtained from the two groups after each region has been seeded, as well as on the corresponding diffusion depth t_{crit} obtained for each node seeding and each group. In the case of the full 90 nodes networks, the *R* *t*-statistics is insignificant, with -0.77 std and $p=0.44$ ($p_{fdr}=0.44$). On the other hand, the diffusion depth t_{crit} at which a maximum *R* is reached yields -2.61 std with $p=9.7\times10^{-3}$ ($p_{fdr}=1.9\times10^{-2}$). When only the ipsilateral hemisphere is considered, we obtain a significant value for *R*, 4.42 std ($p=2.9\times10^{-5}$, $p_{fdr}=5.6\times10^{-5}$) and a nearly significant value for t_{crit}, 1.96 std ($p=5.3\times10^{-2}, p_{fdr}=5.3\times10^{-2}$).

The effect of choice of connectivity measure

The SC network is typically constructed using one of three measures (Iturria-Medina et al., 2007): anatomical connection strength (ACS); anatomical connection density (ACD); and anatomical connection probability (ACP), used in this work. All three SC measures yield comparable results. For comparison purposes, the SC measures are implemented in the graph diffusion model for the TLE-MTS full network case. Figure 8 depicts the results, with the upper left plot giving the *R* resulting from a graph diffusion at each node for the ACD case. Similar steps are followed for the cases ACP (top right) and ACS (bottom left). A scatter plot of the *R* values obtained from ACS versus those obtained from ACP reveals a nearly straight line (Fig. 8 bottom right). In addition, the *R* values obtained from ACS and ACP are themselves highly correlated, with $R=0.976$.

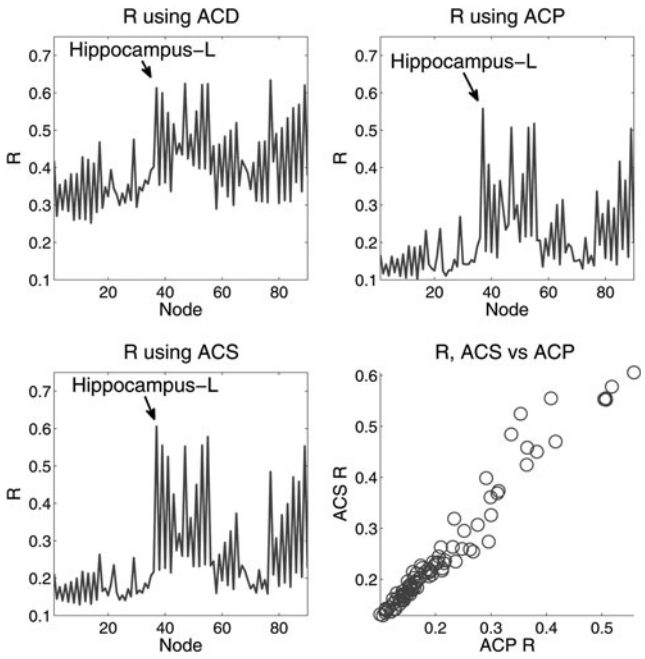

FIG. 8. Implementing three types of SC anatomical connection to the graph diffusion model in the case of TLE-MTS. While all three cases give similar results, the *R* values obtained from ACS and ACP are highly correlated ($R=0.976$). ACS, anatomical connection strength; ACP, anatomical connection probability.

Discussion

Summary of main results

A graph diffusion-based model of progressive deafferentation in epilepsy is proposed, employing a simple first-order differential equation constrained on the structural network. The model assumes that the topography of neuronal loss is a result of the network-wide effect of progressive deafferentation by a diffusive spread process restricted to the network and seeded at the epileptogenic onset zone, for example, hippocampus in TLE-MTS. Our model is essentially a mathematical encoding of this progressive deafferentation, which is assumed to be mediated by loss of trophic support, axonal reaction, and retrograde and anterograde degeneration. The model was validated by computing the Pearson correlation between patients' regional MD as a surrogate of neuronal loss, and the model was evaluated at all diffusion time points for each region.

The TLE-MTS estimate gives a strong resemblance to measured group-level MD from 10 TLE subjects. Due to its highly localized neuronal loss (ipsilateral hippocampus), TLE-MTS yields the best prediction with high correlation metric *R* (Fig. 2c, d). TLE-MTS shows strong validation of our model, where the proposed graph diffusion estimates are highly correlated with group-level *t*-statistics and appear

to be consistent with similar conclusions reached in the literature. A higher Pearson correlation is obtained when we consider only the ipsilateral cortex hemisphere (Fig. 4).

The heterogeneity of the TLE-no case leads to lower R values when evaluated on the entire cortex for all nodes. The highest R is obtained when the contralateral calcarine sulcus is seeded. From the observed prominence of occipital and contralateral regions, it appears likely that TLE-no represents a heterogeneous and nonfocally seeded disease, which involves temporal cortices prominently, but not exclusively. When only the ipsilateral hemisphere is considered, the inferior temporal gyrus stands out as a possible epileptogenic focus, a likely onset region, as suggested in Mueller and associates (2009). The resulting TLE-no estimate when the SC is restricted only to the ipsilateral hemisphere may be due to both the tendency of TLE-no to spread in both hemispheres and the limitations of the current methods of estimating SC where the resulting network has the hemispheres typically weakly connected.

The proposed model has only one degree of freedom, t. Despite, or perhaps thanks to, the model's simplicity, it is possible to capture large-scale patterns (in our case, neuronal loss distribution) of such a complex system as the brain, requiring only the SC of a healthy subject. This suggests that it is possible to reduce the complex spatiotemporal dynamics of network-based progressive deafferentation and resultant neuronal loss to a low-dimensional model. The model's simplicity leads to a fast implementation with minimal computational power.

The presented results support the feasibility and suitability of network diffusion as a model of epilepsy-induced neuronal loss. Although the GD model was tested here on group-level MD statistics of relatively homogeneous epilepsy subtypes with stereotyped topography, they support a role, in future work, for the model in clinically relevant analysis of individual epilepsy patients. The quantitative and deterministic nature of the model could in the future make it possible to predict an individual subject's neuronal loss patterns. It might become possible to provide more accurate personalized prognosis regarding likely cognitive, motor, and other deficits. Ideally, given the subject's current state, the model can help identify the network edges through which epilepsy-related influences would most strongly spread, which could provide invaluable information during surgery preparation. This is the motivation for our work and will be addressed in future studies. The linearity of the proposed method makes it possible to invert the diffusion process, which could potentially enable inferring the epileptogenic focus from the patient's measured atrophy patterns.

In addition to MD, many other diffusion-related measures have been proposed, including fractional anisotrophy (FA) and radial (RD) and axial (AD) diffusivity. It is possible that some of these alternate measures might also be appropriate for the purpose at hand. Our choice of MD was driven by the fact that it is not dependent on fiber orientation, which is less useful as a measure of neuronal integrity than in WM where orientation is a key element. AD has a similar dependence on orientation. However, RD might be an interesting measure to test in the future, as it is presumably exclusive of orientational aspects of diffusion, and might therefore form a reasonable measure of neuronal integrity in GM.

Neuronal loss and GD model prediction

The hippocampus is highly connected with regions of the parietal lobe, particularly the precuneus, posterior cingulate, and bilateral inferior parietal regions. Thus deafferentation in TLE-MTS could plausibly lead to neuronal loss in the parietal lobe (Bettus et al., 2009), as confirmed by our GD model, which predicts strong neuronal loss in the ipsilateral parietal lobe and especially the precuneus.

Related to Mueller and associates (2009), the model predicts widespread TLE-MTS neuronal loss in the ipsilateral temporal lobe (fusiform, parahippocampal), in agreement with McDonald and associates (2008). In addition, the GD model predicts neuronal loss in the ipsilateral inferior and middle temporal gyri, ipsilateral lateral orbital frontal gyrus, and ipsilateral lingual gyrus. The model also predicts significant neuronal loss in ipsilateral the subcortical structure, particularly in the thalamus, putamen, and the hippocampus.

The model predicts additional neuronal loss in the frontal lobe, especially in the ipsilateral olfactory bulb, the inferior orbitofrontal gyrus, and the insula cortex. Bernahrdt and associates (2008) report neuronal loss in the temporal lobe, as subsequently confirmed in Mueller and associates (2009), but also in the frontal lobe (Lin et al., 2007) where it is proposed that under certain conditions, mesiotemporal epilepsy activities would propagate through the thalamus to the frontocentral areas. Related to the findings in Mueller and associates (2009), it is found that the frontal and parietal regions play a crucial role in the evolution of complex partial seizure (Englot and Blumenfeld, 2009), likely contributing to the atrophies predicted in the same regions by the proposed GD model.

TLE-no epilepsy has, in general, different atrophy distribution from its TLE-MTS counterpart. In this work, GD over the entire GM nodes gives the contralateral calcarine as an epilepsy focus candidate for seed diffusion, leading to the highest R with MD abnormalities. Given the heterogeneity in epilepsy origin in TLE-no, it is unlikely that this is the best, or the only seed for our model. The correlation coefficient itself is rather weak. Another explanation of the low TLE-no R is the limited long-range connectivity obtained from the SC matrix needed for the GD model.

While analysis over the whole GM yielded limited correlation with the t-statistics, confining the analysis only to the ipsilateral hemisphere yielded results that are more in line with published literature. It is shown in Scanlon and associates (2013); Mueller and associates (2007, 2009); and Carne and associates (2007) using FA abnormalities that TLE-no anomalies are consistently found in the frontal lobe regions, including the insula, in addition to the ipsilateral inferior temporal gyrus. In the network of the ipsilateral hemisphere, the GD seeded at the inferior temporal gyrus yields the highest R as shown in TLE-no Mean Diffusivity Section. This is consistent with the MD abnormality findings of the GD model in the frontal lobe (inferior orbitofrontal gyrus, rolandic operculum, olfactory bulb, and insula), as well as the inferior temporal gyrus. Unlike TLE-MTS where the MD abnormalities stand out mainly in the ipsilateral hemisphere and thus lead to a better estimate of the MD abnormalities spread, the TLE-no case tends to spread across the hemispheres.

The proposed model suggests that neuronal loss due to epilepsy is driven by GD in the structural network, modeled by the symmetric normalized Laplacian. The Laplacian matrix

L's eigenvector can capture an approximate presentation of the neuronal loss due to TLE. For example, the eigenmode $|\mathbf{u}_2|$ corresponding to a small eigenvalue gives a correlation of $R = 0.363$, approximating the TLE-no MD abnormality. Interestingly, eigenmode $|\mathbf{u}_{78}|$ captures neuronal loss at the hippocampus as well as at the inferior temporal gyrus, a region considered a candidate for TLE-no epileptogenic focus (Mueller et al., 2009). Performing similar analysis with the TLE-MTS t-statistics gives eigenmode $\mathbf{u}_{78}$ as the one with highest R.

Relationship to current work in brain network analysis

The GD model proposed in this work is closely related to a family of techniques adopted in the areas of signal and image processing (Elmoataz et al., 2008; Zhang and Hancock, 2008). Elmoataz and associates (2008) proposed a GD model for image enhancement using weighted graphs. Image smoothing methods based on heat kernels and weighted undirected graphs have been proposed in Zhang and Hancock (2008). Bougleux and associates (2007) developed image smoothing and denoising approaches based on Laplacian operators. Shuman and associates (2013) gave an excellent general discussion of graph signal and image processing. Our laboratory developed a similar network model reflecting macroscopic evolution of neurodegenerative brain diseases (Raj et al., 2012). A similar graph diffusion model was also successful in capturing the relationship between structural and functional connectivities.

The fact that seemingly distinct brain processes such as neurodegenerative spread to functional networks to epilepsy are captured by a simple GD model indicates a probable convergence in large scale brain patterns, at least, as a first-order approximation. A clue to this convergent behavior comes from the recurring role of certain common elements in many neurological diseases; for instance, medial temporal area and the hippocampus play a central role in both Alzheimer's dementia and TLE.

This study is also related to the larger and higher topical interest in graph theory as an analysis tool for brain networks, as well as focused application in epilepsy. A recent review of graph theory and its application summarizes the usefulness in brain network analysis (Reijneveld et al., 2007; Telesford et al., 2011). Another review of networks application to brain functional and structural graphs discusses brain connectivity viewed as a small-world network (Bassett and Bullmore, 2006). The authors discuss the mathematical theory underlying small world analysis and examine how it translates as a quantification tool of connectivity matrices.

A review of network theory application to epilepsy (Lemieux et al., 2011) sheds light on functional and structural networks analysis and the challenges arising from analyzing epilepsy-disrupted networks. In particular, network models have been successfully applied to epilepsy where, for example, Bernhardt and associates (2011) use graph analysis of cortical thickness to show that TLE subjects exhibit brain networks with altered topology. Moreover, the authors find increased path length and clustering in TLE subjects. In a related work, Raj and associates (2010) confirm prior findings using networks methods that, significant focal thinning in the ipsilateral temporal lobe for the case of TLE-MTS exhibits weaker and more widespread bilateral thinning. They additionally develop new network metrics that lead to enhanced discrimination of the type of epilepsy.

Alterations in functional connectivity during interictal state have been observed in TLE patients (Sequeira et al., 2013), and a reduced activity is observed in the default mode network in those with epilepsy disorder (Zhang et al., 2010). In addition, Sequeira and associates (2013) observed an increased connectivity in the medial temporal lobe and in several subcortical structures, while finding a reduced connectivity in distant cortical structures. The reduced baseline activity may be a compensatory mechanism to reduce the risk of seizure and excitotoxicity, although it may contribute to deafferentation. Also, the seizure activity has been shown to cause a decoupling of structural versus functional connectivity (Zhang et al., 2010). Network alterations have been observed to promote the onset of future seizures through the formation of pro-TLE kainatergic synapses (Ben-Ari et al., 2008).

Long-term exposure to TLE leads to a progressive worsening in functional as well as structural connectivities. For example, van Dellen and associates (2009) performed graph analysis on the electrocorticography of temporal lobe surgery patients and concluded that functional connectivity networks in the ipsilateral temporal lobe exhibit increased randomness in the subjects with a longer history of epilepsy. Similarly, Zhang and associates (2010) in a study of idiopathic generalized epilepsy show that function and structure networks are less than optimal and exhibit altered connectivities in both cortical and subcortical regions. Our work is different from these studies, which are phenomenological description of network alterations in epilepsy. In contrast, we attempt, in this study, a specific model of network-based progressive deafferentation starting from first principles.

Clinical applications

Although validation was performed, in this study, on group-level neuronal loss statistics of homogeneous epilepsy subtypes with stereotyped topography, they support a role for the model in clinically relevant analysis of individual epilepsy patients. In addition to the scientific question of resolving the mechanism of spread of epilepsy in the brain, eventual clinical applications were the motivation for our work. Some of these applications are listed in this study, and will be addressed in future studies.

Since the model is quantitative and deterministic, it may in the future be used as a predictive tool in determining future patterns of neuronal loss in a subject, based on their current pattern. It might become possible to provide more accurate personalized prognosis regarding likely cognitive, motor, and other deficits. Given the subject's current state, the model can help identify the network edges through which epilepsy-related influences would most strongly spread, which could provide invaluable information during surgery preparation. The linearity of the proposed method makes it possible to invert the diffusion process, which in turn could enable estimation of the epileptogenic focus of a patient's brain. Thus, the model can be reversed, starting with the neuronal loss distribution, to estimate the epileptogenic focus in a given patient without the need for the intracranial EEG step. This can potentially help streamline the decision as to whether a given TLE patient makes a good candidate for surgery.

Properly validated quantitative models of spread have the potential to become indispensable tools in clinical care and

management, for instance, as a predictive tool for assessing a patient's likely future topography of neuronal loss and potential for cognitive/motor impairment. Such a tool could allow identification of the seizure onset zone and other regions of epileptogenic activity—important clinical questions during surgery planning. Much of this research is phenomenological and descriptive, hence not well suited as quantitative tools. Quantitative model development is further hampered by heterogeneity in the topography of the disease among TLE patients. Although this study was restricted to group analysis as a means of testing the proposed models, our approach is completely applicable to single-subject analysis, in which case it would benefit from the individual patient's unique connectome and neuronal loss profiles. Thus, the proposed method could be applicable even in heterogeneous epilepsies, for instance, frontal lobe epilepsy of diverse etiology.

Study limitations

Limitations of neuroimaging data processing, including MD and diffusion MRI-derived tractography, means that SC between topologically distant regions are underweighted and sometimes unreliable, especially interhemispheric connections. Validity of the proposed graph diffusion model depends on the accuracy of SC. As a result, the model underestimates contralateral abnormality as is clearly shown in the TLE-no abnormality estimate, where the graph diffusion over the entire network misses the likely focus, but captures it when the structural network is limited to the ipsilateral hemisphere. An additional limitation is the use of different scanners in the healthy connectome scans and TLE subjects, however, for the purpose of obtaining regional MD, *t*-statistics healthy controls and TLE patients were acquired on the same scanner.

The connectome scans involving high angular resolution DTI were performed separately on a different healthy cohort on a different scanner, but these data are not directly compared to TLE data at any stage during the presented analysis. Another limitation of this study is that it does not take into account the feedback mechanism between structure and function, where progressive neuronal damage has a functional correlate, and consequent change in structure leads to an alteration in function. The presented validation study was confined to group-level neuronal loss statistics, as a consequence, we were only able to include in our analysis the epilepsy subtypes TLE-MTS, which has stereotyped topographic distributions, and TLE-no.

Materials and Methods

Network notation

In a brain network, each node represents a GM region located on either the neocortex or in deep brain subcortical areas. We define a network $G=V,E$ with a set of N nodes given by $V=\{v_i|i\in 1,\ldots,N\}$ and a set of edges given by an ordered node pair $E=\{(i,j)|i\in V, j\in V\}$ (Chung, 1997). Between any two nodes i and j, there might exist a fiber pathway whose connectivity weight $c_{i,j}\in[0,\infty)$ can be measured from dMRI tractography, and this defines a connectivity matrix $C=\{c_{i,j}|(i,j)\in E\}$. Although some individual neurons are known to be directional, dMRI does not allow measurement of directionality. Major fiber bundles resolvable by dMRI, especially corticocortical pathways, are generally bidirectional, having roughly equal number of connections in either direction (Albright, 1984). We define the *connectivity strength* or the *weighted degree* of a node i in this graph as the sum of all connection weights:

$$\delta_i=\sum_{j|(i,j)\in E} c_{i,j}. \quad (1)$$

Table 2 describes the various parameters and variables used in this work.

A network diffusion model for epilepsy

Spread of neuronal loss. We propose a simple linear model, which assumes that neuronal loss is a propagation event triggered at an onset zone by excitotoxicity or other events. The neuronal loss then spreads throughout the brain network through a degenerative process modulated by loss of trophic support, axonal reaction, and retrograde as well as anterograde degeneration. We model this hypothesis as a dynamic process enacted on the structural network This choice precludes investigation of the effect of dynamically changing network connectivity and simply assumes a static intact network. Clearly, these assumptions are going to become inapplicable in advanced cases with widespread and strong atrophy.

We assume that a single event entailing loss of x_1^0 neurons per voxel in an isolated region $R1$ triggers internal (to the region) degenerative dynamics given by $x_1(t)=x_1^0\exp(-\beta t)$. This is then the ''impulse response'' of the region and simply encodes the fact that a single insult will cause further degeneration, persisting in the region with a half-life of $1/\beta$. This corresponds to a simple damped system described by $dx_1(t)/dt=-\beta x_1(t)$. Next, consider a *pair* of cortical regions $R1$ and $R2$, whose connectivity weight is $c_{1,2}$. In a short time interval δt, let the number of newly deceased neurons in $R2$ be N_2x_2, where N_2 is the number of voxels in $R2$. This group of external newly deceased neurons then triggers degeneration in $R1$, modeled as a Poisson process. Accounting for

Table 2. Summary of the Variables and Definitions Used in This Text

Parameter or variable	*Role*
G	Structural network of N nodes
V	Set of nodes of G
v_i	ith node of G
E	Set of edges of G
C	SC matrix
$c_{i,j}$	Element (i,j) of C
δ_i	Weighted degree of node i
L	Laplacian of C
λ_i	ith eigenvalue of L
$\mathbf{u}_i$	ith eigenvector of L
Δ	Diagonal degree matrix of L
β	Diffusion rate
$x_i(t)$	Neuronal loss in the i region
N_i	No. of voxels in ith region Ri
Φ	Atrophy spread due to neuronal loss

SC, structural connectivity.

both the internal and externally induced neuronal loss dynamics in $R1$, we have

$$\frac{dx_1(t)}{dt} = \beta\left(\frac{1}{N_1}c_{1,2}\frac{1}{\delta_2}N_2x_2(t) - x_1(t)\right), \quad (2)$$

where we assume identical rate constant β for both the internal and external neuronal loss dynamics for simplicity. For multiple afferent into $R1$, we modify Equation (2) to

$$\frac{dx_i(t)}{dt} = \beta\left(\frac{1}{N_i}\sum_j c_{i,j}\frac{1}{\delta_j}N_jx_j(t) - x_i(t)\right). \quad (3)$$

Now, assuming a relationship between GM volume N_k and ith node degree δ_i given by $N_k \propto \sqrt{\delta_k}\ \forall\kappa\in \mathrm{V}$, we have

$$\frac{dx_i(t)}{dt} = \beta\left(\delta_i^{-\frac{1}{2}}\sum_j c_{i,j}\delta_j^{-\frac{1}{2}}x_j(t) - x_i(t)\right). \quad (4)$$

On the entire network, Equation (4) can be compactly expressed as

$$\frac{d\mathrm{x}(t)}{dt} = -\beta \mathrm{L}\mathrm{x}(t), \quad (5)$$

where $\mathbf{x}(t)$ is an $N\times 1$ vector describing the fraction of epileptogenic neurons in all brain regions, and matrix L is the well-known symmetric and normalized Laplacian

$$\mathrm{L} = I - \Delta^{-\frac{1}{2}}\mathrm{C}\Delta^{-\frac{1}{2}},$$

where Δ is the diagonal degree matrix with the node degree δ_i as the ith diagonal element. Equation (5) admits a closed form solution $\mathrm{x}(t) = \exp(-\beta \mathrm{L}t)\mathrm{x}_0$, giving a time-dependent process starting with initial ''seed'' map $\mathrm{x}_\mathbf{0}$ at $t=0$ and ending at a uniform distribution at $t=\infty$, such that eventually all regions degenerate at the same constant rate. Since $\mathrm{x}(t)$ denotes the number of newly deceased neurons at any instant, the overall neuronal loss during the degenerative process is given by the time integral

$$\Phi(t) \propto \int_0^t \mathrm{x}(\tau)d\tau, \quad (6)$$

which has a closed form solution

$$\Phi(t) = \frac{1}{\beta}\sum_{i=1}^{K}\frac{1}{\lambda_i}(1 - \exp(-\beta\lambda_i t))\mathbf{u}_i\mathbf{u}_i^1, \mathrm{x}_0, \quad (7)$$

$\Phi(t)$ is a function of time, where time has units of years since the model captures the slow spread of degenerating neurons. Since the true time since onset is not empirically accessible in general, in Results Section we will estimate the diffusion time as the instant t_{crit} when the theoretical pattern $\Phi(t)$ best matches measured neuronal loss pattern in the subject. Both t_{crit} and the rate constant β are *a priori* inaccessible and must be empirically determined by data fitting. Seed vector x_0 is known in the TLE-MTS case to a high level of confidence since prominent hippocampal sclerosis indicates a high likelihood that it is indeed the focus location. Thus, we initialize x_0 by a unit vector, which is zero except for the element corresponding to the hippocampus node, which is 1. Details of relevant network theory can be found in Chung (1997).

Study TLE population

Three groups consisting of 11 TLE-no subjects, 10 TLE-MTS subjects, and 35 healthy subjects were recruited. Subjects underwent scanning on a Siemens Allegra 3T scanner at New York University Center for Brain Imaging. All participants had a T1-weighted MRI sequence optimized for gray-WM contrast. (TR = 2530 ms, TE = 3.25 ms, T1 = 1100 ms, flip angle = 7°, field of view (FOV) = 256 mm, matrix = $256\times 256\times 192$, voxel size = $1\times 1.33\times 1.33\,\mathrm{mm}^3$). Images were corrected for nonlinear warping caused by nonuniform fields created by the gradient coils. The DTI volumes were segmented and atlased into 90 regions using SPM 8 (Friston et al., 2007), and masks defining GM and WM were obtained. Finally, the MD over all the GM 90 regions was obtained. Table 3 lists the demographics of all three groups.

Regarding the TLE-MTS group, the mean age differs from the healthy and TLE-no groups due to the availability of subjects with both T1 and DTI data. However, this does not seem to adversely impact the proposed models performance as the prediction matches published work on TLE-MTS (Riederer et al., 2008; Spencer, 2002).

Connectome matrices from healthy cohorts

SC matrices were obtained from eight subjects. The subjects' ages range from 23 to 60, with three females and five males. Subjects were scanned under normal subject protocol approved by the institutional review board (IRB). Table 3 gives the demographics of the connectome group.

T1-weighted structural MR and high angular resolution diffusion imaging (HARDI) data were collected on eight healthy adults on a 3T GE Signa EXCITE scanner (GE Healthcare, Waukesha, WI). HARDI data were acquired using 55 isotropically distributed diffusion-encoding directions at $b = 1000\,s/\mathrm{mm}^2$ and one at $b = 0\,s/\mathrm{mm}^2$, acquired at 72 1.8 mm thick interleaved slices with no gap between slices and 128×128 matrix size that was zero-filled during reconstruction to 256×256 with an FOV of 230 mm. The structural scan was an axial 3D inversion recovery fast spoiled gradient recalled echo (FSPGR) T1-weighted protocol (TE = 1.5 msec, TR = 6.3 msec, TI = 400 msec, flip angle of 15) with 230 mm FOV and 156 1.0 mm contiguous partitions at a 256×256 matrix.

Structural and diffusion MR volumes were coregistered using SPM tools in MATLAB (Alemán-Gómez et al., 2006; Friston et al., 1994), and then parcellated into 90 cerebral cortical structures as per Tzourio-Mazoyer and associates (2002). Parcellated regions were used to seed probabilistic tractography in coregistered diffusion MRI volumes. Connectivity weight between any two regions was given by a weighted sum of tracts going between them, as per Iturria-Medina and associates (2007). Simple statistical thresholding was performed to remove spurious weak connections,

TABLE 3. SUBJECTS' DEMOGRAPHICS

Group	*Gender (F/M)*	*Age*
Connectum	3/5	35 ± 13
Healthy	18/17	39 ± 13
TLE-MTS	5/5	29 ± 11
TLE-no	6/5	35 ± 14

defined as those below the $p=0.001$ level of significance. Probabilistic masks, including both white and GM, were obtained. At $p>0.001$, the thresholded network has 11.56 nonzero connections. Threshold level $p>0.001$ has been previously reported in Ivković and associates (2012). Since the proposed diffusion model is linear, a change in p should not adversely affect the model's prediction. A voxel was included in the mask if both its GM and WM probabilities exceeded 0.5.

Acknowledgment

A.R. and F.A. were supported by the NIH grant R01 NS075425.

Author Disclosure Statement

No competing financial interests exist.

References

Abdelnour F, Voss H, Raj A. 2014. Network diffusion accurately models the relationship between structural and functional brain connectivity networks. NeuroImage 90:335–347.

Albright TD. 1984. Direction and orientation selectivity of neurons in visual area MT of the macaque. J Neurophysiol 52:1106–1130.

Alemán-Gómez Y, Melie-Garca L, Valdés-Hernandez P. 2006. IBASPM: Toolbox for automatic parcellation of brain structures In: *12th Annual Meeting of the Organization for Human Brain Mapping*. June 11–15, 2006.

Ashby FG. 2011. *Statistical Analysis of fMRI Data.* Cambridge, MA: MIT Press.

Assaf BA, Mohamed FB, Abou-Khaled KJ, Williams JM, Yazeji MS, Haselgrove J, Faro SH. 2003. Diffusion tensor imaging of the hippocampal formation in temporal lobe epilepsy. Am J Neuroradiol 24:1857–1862.

Bartolomei F, Khalil M, Wendling F, Sontheimer A, Régis J, Ranjeva JP, et al. 2005. Entorhinal cortex involvement in human mesial temporal lobe epilepsy: an electrophysiologic and volumetric study. Epilepsia 46:677–687.

Bassett DS, Bullmore E. 2006. Small-world brain networks. Neuroscientist 12:512–523.

Ben-Ari Y, Crepel V, Represa A. 2008. Seizures beget seizures in temporal lobe epilepsies: the boomerang effects of newly formed aberrant kainatergic synapses. Epilepsy Curr 81:68–72.

Bernhardt BC, Chen Z, He Y, Evans AC, Bernasconi N. 2011. Graph-theoretical analysis reveals disrupted small-world organization of cortical thickness correlation networks in temporal lobe epilepsy. Cereb Cortex 21:2147–2157.

Bernhardt BC, Worsley KJ, Besson P, Concha L, Lerch JP, Evans AC, Bernasconi N. 2008. Mapping limbic network organization in temporal lobe epilepsy using morphometric correlations: insights on the relation between mesiotemporal connectivity and cortical atrophy. NeuroImage 42:515–524.

Bertram EH. 2009. Temporal lobe epilepsy: where do the seizures really begin? Epilepsy Behav 14:32–37.

Bettus G, Guedj E, Joyeux F, Confort-Gouny S, Soulier E, Laguitton V, et al. 2009. Decreased basal fMRI functional connectivity in epileptogenic networks and contralateral compensatory mechanisms. Hum Brain Mapp 30:1580–1591.

Bonilha L, Edwards JC, Kinsman SL, Morgan PS, Fridriksson J, Rorden C, et al. 2010. Extrahippocampal gray matter loss and hippocampal deafferentation in patients with temporal lobe epilepsy. Epilepsia 51:519–528.

Bougleux S, Elmoataz A, Melkemi M. 2007. Discrete regularization on weighted graphs for image and mesh filtering. In: Sgallari F, Murli A, Paragios N (eds.), *Scale Space and Variational Methods in Computer Vision*: First International Conference. Berlin, Heidelberg: Springer Berlin Heidelberg, pp. 128–139.

Bozzali M, Cercignani M, Sormani MP, Comi G, Filippi M. 2002. Quantification of brain gray matter damage in different MS phenotypes by use of diffusion tensor MR imaging. Am J Neuroradiol 23:985–988.

Carne R, O'Brien T, Kilpatrick C, MacGregor L, Litewka L, Hicks R, Cook M. 2007. 'MRI-negative PET-positive' temporal lobe epilepsy (TLE) and mesial TLE differ with quantitative MRI and PET: a case control study. BMC Neurol 7:16.

Chung FRK. 1997. *Spectral Graph Theory* Number 92 in Regional Conference Series in Mathematics. AMS.

Concha L, Beaulieu C, Collins DL, Gross DW. 2009. White-matter diffusion abnormalities in temporal-lobe epilepsy with and without mesial temporal sclerosis. J Neurol Neurosurg Psychiatry 80:312–319.

Concha L, Kim H, Bernasconi A, Bernhardt BC, Bernasconi N. 2012. Spatial patterns of water diffusion along white matter tracts in temporal lobe epilepsy. Neurology 79:455–462.

DuBois J, Devinsky O, Carlson C, Kuzniecky R, Quinn B, Alper K, et al. 2011. Abnormalities of cortical thickness in postictal psychosis. Epilepsy Behav 21:132–136.

Elmoataz A, Lezoray O, Bougleux S. 2008. Nonlocal discrete regularization on weighted graphs: a framework for image and manifold processing. IEEE Trans Image Process 17:1047–1060.

Englot DJ, Blumenfeld H. 2009. Consciousness and epilepsy: why are complex-partial seizures complex? In: Steven Laureys NDS, Owen AM (eds.), *Coma Science: Clinical and Ethical Implications*, Vol. 177 of *Progress in Brain Research.* Elsevier; pp. 147–170.

Fisher RS, Acevedo C, Arzimanoglou A, Bogacz A, Cross JH, Elger CE, et al. 2014. A practical clinical definition of epilepsy. *Epilepsia* 54: 475–482.

Friston K, Ashburner J, Kiebel S, Penny W, eds. 2007. *Statistical Parametric Mapping: The Analysis of Functional Brain Images.* London: Academic Press.

Friston K, Holmes A, Worsley K, Poline JP, Frith CD, Frackowiak RSJ. 1994. Statistical parametric maps in functional imaging: a general linear approach. Hum Brain Mapp 2:189–210.

Gotman J, Levtova V. 1996. Amygdala-hippocampus relationships in temporal lobe seizures: a phase-coherence study. Epilepsy Res 25:51–57.

Hirtz D, Thurman D, Grwinn-Hardy K, Mohamed M, Chaudhuri A, Zalutsky R. 2007. How common are the ''common'' neurologic disorders? Neurology 68:326–337.

Iturria-Medina Y, Canales-Rodrguez E, Melie-Garca L, Valdés-Hernández P, Martínez-Montes E, Alemán-Gómez Y, Sánchez-Bornot J. 2007. Characterizing brain anatomical connections using diffusion weighted MRI and graph theory. NeuroImage 36:645–660.

Ivković M, Kuceyeski A, Raj A. 2012. Statistics of weighted brain networks reveal hierarchical organization and gaussian degree distribution. PLoS One 7:e35029.

Keller SS, Schonene-Bake JC, Gerdes JS, Weber B, Deppe M. 2012. Concomitant fractional anisotropy and volumetric abnormalities in temporal lobe epilepsy: cross-sectional evidence for progressive neurologic injury. PLoS One 7:e46791.

Lemieux L, Daunizeau J, Walker MC. 2011. Concepts of connectivity and human epileptic activity. Front Syst Neurosci 5:12.

Lin JJ, Salamon N, Lee AD, Dutton RA, Geaga JA, Hayashi KM, et al. 2007. Reduced neocortical thickness and complexity mapped in mesial temporal lobe epilepsy with hippocampal sclerosis. Cereb Cortex 17:2007–2018.

McDonald CR, Hagler DJ, Ahmadi ME, Tecoma E, Iragui V, Gharapetian L, et al. 2008. Regional neocortical thinning in mesial temporal lobe epilepsy. Epilepsia 49:794–803.

Meldrum BS. 1993. Excitotoxicity and selective neuronal loss in epilepsy. Brain Pathol 3:405–412.

Mueller S, Laxer K, Barakos J, Cheong I, Garcia P, Weiner M. 2009. Widespread neocortical abnormalities in temporal lobe epilepsy with and without mesial sclerosis. NeuroImage 46:353–359.

Mueller SG, Laxer KD, Schuff N, Weiner MW. 2007. Voxel-based T2 relaxation rate measurements in temporal lobe epilepsy (TLE) with and without mesial temporal sclerosis. Epilepsia 48:220–228.

Mukherjee P, Berman J, Chung S, Hess C, Henry R. 2008. Diffusion tensor MR imaging and fiber tractography: theoretic underpinnings. Am J Neuroradiol 29:632–641.

Pfefferbaum A, Adalsteinsson E, Rohlfing T, Sullivan EV. 2010. Diffusion tensor imaging of deep gray matter brain structures: effects of age and iron concentration. Neurobiol Aging 31:482–493.

Raj A, Kuceyeski A, Weiner M. 2012. A network diffusion model of disease progression in dementia. Neuron 73: 1204–1215.

Raj A, Mueller S, Young K, Laxer K, Weiner M. 2010. Network-level analysis of cortical thickness of the epileptic brain. NeuroImage 52:1302–1313.

Reijneveld JC, Ponten SC, Berendse HW, Stam CJ. 2007. The application of graph theoretical analysis to complex networks in the brain. Clin Neurophysiol 118:2317–2331.

Riederer F, Lanzenberger R, Kaya M, Prayer D, Serles W, Baumgartner C. 2008. Network atrophy in temporal lobe epilepsy: a voxel-based morphometry study. Neurology 71: 419–425.

Scanlon C, Mueller SG, Cheong I, Hartig M, Weiner MW, Laxer KD. 2013. Grey and white matter abnormalities in temporal lobe epilepsy with and without mesial temporal sclerosis. J Neurol 260:2320–2329.

Sequeira KM, Tabesh A, Sainju RK, Desantis SM, Naselaris T, Joseph JE, et al. 2013. Perfusion network shift during seizures in medial temporal lobe epilepsy. PLoS One 8:e53204.

Shuman DI, Narang SK, Frossard P, Ortega A, Vandergheynst P. 2013. The emerging field of signal processing on graphs: extending high-dimensional data analysis to networks and other irregular domains. *IEEE Signal Processing Magazine* pp. 83–98.

Spencer SS. 2002. Neural networks in human epilepsy: evidence of and implications for treatment. Epilepsia 43:219–227.

Stafstrom CE. 2005. The role of the subiculum in epilepsy and epileptogenesis. Epilepsy Curr 5:121–129.

Sutula TP, Hagen J, Pitkanen A. 2003. Do epileptic seizures damage the brain? Curr Opin Neurol 16:189–195.

Telesford QK, Simpson SL, Burdette JH, Hayasaka S, Laurienti PJ. 2011. The brain as a complex system: using network science as a tool for understanding the brain. Brain Connect 1:295–308.

Thesen T, Quinn BT, Carlson C, Devinsky O, DuBois J, McDonald CR, et al. 2011. Detection of epileptogenic cortical malformations with surface-based MRI morphometry. PLoS One 6:e16430.

Tzourio-Mazoyer N, Landeau B, Papathanassiou D, Crivello F, Etard O, Delcroix N, et al. 2002. Automated anatomical labeling of activations in SPM using a macroscopic anatomical parcellation of the MNI MRI single-subject brain. NeuroImage 15:273–289.

van Dellen E, Douw L, Baayen JC, Heimans JJ, Ponten SC, Vandertop WP, et al. 2009. Long-term effects of temporal lobe epilepsy on local neural networks: a graph theoretical analysis of corticography recordings. PLoS One 4:e8081.

Zhang F, Hancock ER. 2008. Graph spectral image smoothing using the heat kernel. Pattern Recogn 41:3328–3342.

Zhang Z, Lu G, Zhong Y, Tan Q, Liao W, Wang Z, et al. 2010. Altered spontaneous neuronal activity of the default-mode network in mesial temporal lobe epilepsy. Brain Res 1323: 152–160.

Address correspondence to:
Farras Abdelnour
Department of Radiology
Weill Cornell Medical College
407 E, 61st Street RR110
New York, NY 10021

E-mail: farras.abdelnour@gmail.com